Heavy Higgs Bosons in BSM

Mustafa Ashry
mustafa@sci.cu.edu.eg
Department of Mathematics, Faculty of Science, Cairo University

Based on PhysRevD.107.055044, PhysRevD.104.015016,BSM-2021 Conf. Proc., Eur.Phys.J.C 84 (2024) 433 [4, 9, 3, 5]

Mini Workshop on HHH

July 31, 2024

Outline

1. The LRIS Model
2. Heavy Higgs in LRIS at the LHC
   - $h' \to hh \to b\bar{b}\gamma\gamma$ and $h' \to ZZ \to 4\ell$
   - $H^{\pm}$ Contribution to a_μ
3. Heavy Higgs in BLSSM Model
4. Conclusion

Outline

1. The LRIS Model
2. Heavy Higgs in LRIS at the LHC
   - $h' \to hh \to b\bar{b}\gamma\gamma$ and $h' \to ZZ \to 4\ell$
   - $H^{\pm}$ Contribution to a_μ
3. Heavy Higgs in BLSSM Model
4. Conclusion

Outline

1. The LRIS Model
2. Heavy Higgs in LRIS at the LHC
   - $h' \to hh \to b\bar{b}\gamma\gamma$ and $h' \to ZZ \to 4\ell$
   - $H^{\pm}$ Contribution to a_{μ}
3. Heavy Higgs in BLSSM Model
4. Conclusion

Outline

1 The LRIS Model

2 Heavy Higgs in LRIS at the LHC
- $h' \to hh \to b\bar{b}\gamma\gamma$ and $h' \to ZZ \to 4\ell$
- $H^{\pm}$ Contribution to a_{μ}

3 Heavy Higgs in BLSSM Model

4 Conclusion

Outline

1. The LRIS Model
2. Heavy Higgs in LRIS at the LHC
   - $h' \to hh \to b\bar{b}\gamma\gamma$ and $h' \to ZZ \to 4\ell$
   - $H^{\pm}$ Contribution to a_μ
3. Heavy Higgs in BLSSM Model
4. Conclusion

Outline

1. The LRIS Model
2. Heavy Higgs in LRIS at the LHC
   - $h' \to hh \to b\bar{b}\gamma\gamma$ and $h' \to ZZ \to 4\ell$
   - $H^{\pm}$ Contribution to a_{μ}
3. Heavy Higgs in BLSSM Model
4. Conclusion

Outline

1. **The LRIS Model**
2. Heavy Higgs in LRIS at the LHC
   - $h' \to hh \to b\bar{b}\gamma\gamma$ and $h' \to ZZ \to 4\ell$
   - $H^{\pm}$ Contribution to a_μ
3. Heavy Higgs in BLSSM Model
4. Conclusion

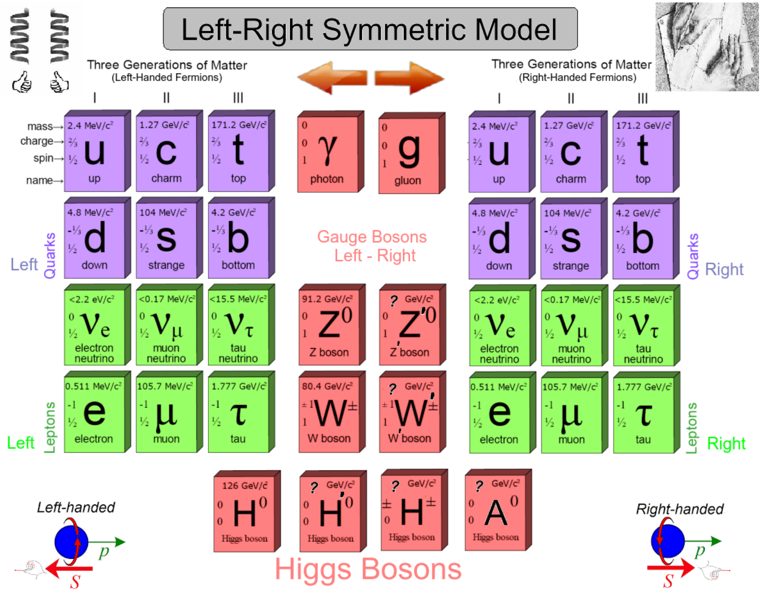
Left-Right Symmetric Model
Three Generations of Matter
(Left-Handed Fermions)
Three Generations of Matter
(Right-Handed Fermions)
I II III
mass→
charge→
spin→
name→
2.4 MeV/c² ⅔ ½ u up
1.27 GeV/c² ⅔ ½ c charm
171.2 GeV/c² ⅔ ½ t top
0 0 1 γ photon
0 0 1 g gluon
4.8 MeV/c² -⅓ ½ d down
104 MeV/c² -⅓ ½ s strange
4.2 GeV/c² -⅓ ½ b bottom
Gauge Bosons
Left - Right
<2.2 eV/c² 0 ½ νe electron neutrino
<0.17 MeV/c² 0 ½ νμ muon neutrino
<15.5 MeV/c² 0 ½ ντ tau neutrino
91.2 GeV/c² 0 1 Z0 Z boson
? GeV/c² 0 1 Z'0 Z' boson
0.511 MeV/c² -1 ½ e electron
105.7 MeV/c² -1 ½ μ muon
1.777 GeV/c² -1 ½ τ tau
80.4 GeV/c² ±1 1 W± W boson
? GeV/c² ±1 1 W'± W' boson
Left Quarks
Quarks Right
Left Leptons
Leptons Right
126 GeV/c² 0 0 H0 Higgs boson
? GeV/c² 0 0 H'0 Higgs boson
? GeV/c² ± 0 H± Higgs boson
? GeV/c² 0 0 A0 Higgs boson
Higgs Bosons
Left-handed
p
S
Right-handed
p
S

Fields	$SU(3)_C \times SU(2)_L \times SU(2)_R \times U_{B-L}$	$\mathbb{Z}_2$
$Q_L = \begin{pmatrix} u_L \\ d_L \end{pmatrix}$	$(\mathbf{3}, \mathbf{2}, \mathbf{1}, \frac{1}{3})$	$+1$
$Q_R = \begin{pmatrix} u_R \\ d_R \end{pmatrix}$	$(\mathbf{3}, \mathbf{1}, \mathbf{2}, \frac{1}{3})$	$+1$
$L_L = \begin{pmatrix} \nu_L \\ e_L \end{pmatrix}$	$(\mathbf{1}, \mathbf{2}, \mathbf{1}, -1)$	$+1$
$L_R = \begin{pmatrix} \nu_R \\ e_R \end{pmatrix}$	$(\mathbf{1}, \mathbf{1}, \mathbf{2}, -1)$	$+1$
S_1	$(\mathbf{1}, \mathbf{1}, \mathbf{1}, -2)$	-1
S_2	$(\mathbf{1}, \mathbf{1}, \mathbf{1}, 2)$	$+1$
$\phi = \begin{pmatrix} \phi_1^0 & \phi_1^+ \\ \phi_2^- & \phi_2^0 \end{pmatrix}$	$(\mathbf{1}, \mathbf{2}, \mathbf{2}, 0)$	$+1$
$\chi_R = \begin{pmatrix} \chi_R^+ \\ \chi_R^0 \end{pmatrix}$	$(\mathbf{1}, \mathbf{1}, \mathbf{2}, 1)$	$+1$

Table 1: The LRIS particle Content quantum numbers.

- The Higgs potential is [7]

$$
\begin{aligned}
V(\phi,\chi_R) = {} & \mu_1 \mathsf{Tr}(\phi^\dagger\phi) + \mu_2[\mathsf{Tr}(\tilde{\phi}\phi^\dagger) + \mathsf{Tr}(\tilde{\phi}^\dagger\phi)] + \lambda_1(\mathsf{Tr}(\phi^\dagger\phi))^2 \\
& + \lambda_2[(\mathsf{Tr}(\tilde{\phi}\phi^\dagger))^2 + (\mathsf{Tr}(\tilde{\phi}^\dagger\phi))^2] + \lambda_3 \mathsf{Tr}(\tilde{\phi}\phi^\dagger)\mathsf{Tr}(\tilde{\phi}^\dagger\phi) \\
& + \lambda_4 \mathsf{Tr}(\phi\phi^\dagger)(\mathsf{Tr}(\tilde{\phi}\phi^\dagger) + \mathsf{Tr}(\tilde{\phi}^\dagger\phi)) + \mu_3(\chi_R^\dagger\chi_R) + \rho_1(\chi_R^\dagger\chi_R)^2 \\
& + \alpha_1 \mathsf{Tr}(\phi^\dagger\phi)(\chi_R^\dagger\chi_R) + \alpha_2(\chi_R^\dagger\phi^\dagger\phi\chi_R) + \alpha_3(\chi_R^\dagger\tilde{\phi}^\dagger\tilde{\phi}\chi_R) \\
& + \alpha_4(\chi_R^\dagger\phi^\dagger\tilde{\phi}\chi_R + h.c.). \qquad (1)
\end{aligned}
$$

- The Yukawa Lagrangian

$$
\begin{aligned}
\mathcal{L}_{\mathsf{Y}} = {} & \sum_{i,j=1}^{3} \bar{L}_{L,i}\big(\phi y^L_{ij} + \tilde{\phi}\tilde{y}^L_{ij}\big)L_{R,j} + \bar{Q}_{L,i}\big(\phi y^Q_{ij} + \tilde{\phi}\tilde{y}^Q_{ij}\big)Q_{R,j} \\
& + \bar{L}_{R,i}\tilde{\chi}_R y^s_{ij} S^c_{2,j} + H.c. \ . \qquad (2)
\end{aligned}
$$

- Spontaneous symmetry breaking (SSB) occurs via the vevs

$$\langle\phi\rangle = \begin{pmatrix} k_1 & 0 \\ 0 & k_2 \end{pmatrix} \sim \mathcal{O}(\text{GeV}), \quad \langle\chi\rangle = \begin{pmatrix} 0 \\ v_R \end{pmatrix} \sim \mathcal{O}(\text{TeV}). \tag{3}$$

and $t_\beta = \tan\beta = k_1/k_2, v = \sqrt{k_1^2 + k_2^2} = 246$ GeV.

- After SSB, the IS neutrino masses Lagrangian is [13, 14, 10, 16]

$$\mathcal{L}_m^\nu = M_D \bar{\nu}_L \nu_R + M_R \bar{\nu}_R^c S_2 + \mu_s \bar{S}_2^c S_2 + h.c., \tag{4}$$

where $M_D = v(y^L s_\beta + \tilde{y}^L c_\beta)/\sqrt{2}$ is the neutrino Dirac mass matrix and $M_R = y^s v_R/\sqrt{2}$.

Outline

1 The LRIS Model

2 Heavy Higgs in LRIS at the LHC
- $h' \to hh \to b\bar{b}\gamma\gamma$ and $h' \to ZZ \to 4\ell$
- $H^{\pm}$ Contribution to a_μ

3 Heavy Higgs in BLSSM Model

4 Conclusion

- Fig. 1 (right) shows the h' decay branching ratios with $m_{h'}$. For $m_{h'} \leq 600$ GeV, BR$(h' \to hh) \geq 10\%$, which gives a hope for probing this heavy Higgs through this channel.

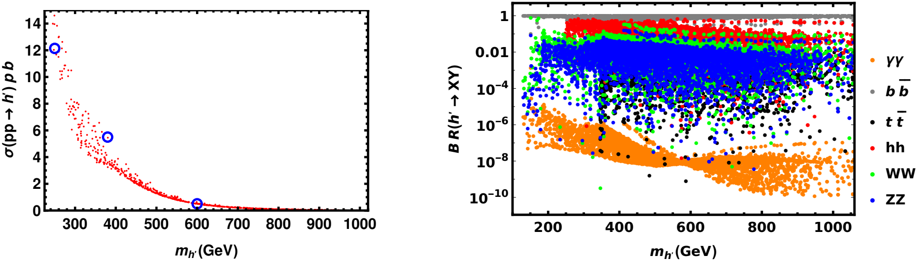

Figure 1: (Left) The h' ggF production cross section with the three BP points circled. (Right) h'-decay branching ratios.

- Here we adapt the following different values of h'-mass: $m_{h'} = 250$ GeV, 400 GeV and 600 GeV

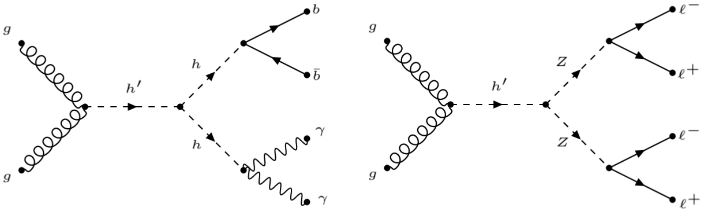

Figure 2: Feynman diagram for the h' ggF production and decay process $gg \to h' \to hh \to b\bar{b}\gamma\gamma$ and $gg \to h' \to ZZ \to 4\ell$.

- We have $\Gamma_{h'}/m_{h'} \ll 1$ and in the narrow width approximation the total cross sections are decomposed into

$$\sigma(pp \to h' \to hh \to b\bar{b}\gamma\gamma) \approx \sigma(pp \to h') \times \mathrm{BR}(h' \to hh) \times \mathrm{BR}(h \to b\bar{b}) \times \mathrm{BR}(h \to \gamma\gamma),$$
$$\sigma(pp \to h' \to ZZ \to 4\ell) \approx \sigma(pp \to h') \times \mathrm{BR}(h' \to ZZ) \times (\mathrm{BR}(Z \to 2\ell))^2$$

$m_{h'}$ (GeV)	$\sigma(pp \to h')$ (pb)	$\mathrm{BR}(h' \to hh)$	$\sigma(pp \to h' \to hh \to b\bar{b}\gamma\gamma)$ (fb)
250	12.140	0.30	6.30
400	5.050	0.20	1.01
600	0.504	0.18	0.05

Table 2: $pp \to h' \to hh \to b\bar{b}\gamma\gamma$ production and decays.

$m_{h'}$ (GeV)	$\sigma(pp \to h')$ (pb)	$\mathrm{BR}(h' \to ZZ)$	$\sigma(pp \to h' \to ZZ \to 4\ell)$ (fb)
250	12.140	0.050	0.2428
400	5.050	0.025	0.0579

Table 3: $pp \to h' \to ZZ$ production and its decay.

The relevant backgrounds are

$$pp \to bbh\gamma\gamma/bbja/bbjj/cc\gamma\gamma/ccj\gamma/jj\gamma\gamma/ggh\gamma\gamma/tt/tt\gamma/tth\gamma\gamma/bbz\gamma\gamma/zh\gamma\gamma.$$

Cuts (Select)	Signal (S): $m_{h'} = 250\ (400)$ GeV	Background (B)	S/$\sqrt{\text{B}}$
Initial (no cut)	$1904.00\ (308.00)$	25058.00	$12.000\ (1.95)$
$(M_{\gamma\gamma})^{<125.0\text{ GeV}}_{>119.5\text{ GeV}}$	$522.00 \pm 19.30\ (106.60 \pm 8.36)$	387.40 ± 19.20	$26.53 \pm 0.01\ (5.42 \pm 0.01)$

Table 4: Cut flow for $h' \to hh \to b\bar{b}\gamma\gamma$ at 300 fb^{-1} and $\sqrt{s} = 14$ TeV for $m_{h'} = 250$ GeV $(400$ GeV$)$.

Cuts (Select)	Signal (S): $m_{h'} = 600$ GeV	Background (B)	S/$\sqrt{\text{B}}$
Initial (no cut)	155.000	250589.00	0.310
$M_{bb} < 200.0$ GeV	52.250 ± 5.18	39823.60 ± 82.40	0.264 ± 0.0008
$(M_{\gamma\gamma})^{<140.0\text{ GeV}}_{>119.5\text{ GeV}}$	34.432 ± 5.91	1826.60 ± 42.00	0.800 ± 0.0004
$(\Delta R)^{bb<2.0}_{\gamma\gamma<2.0}$	28.300 ± 4.46	198.63 ± 7.66	2.010 ± 0.0200
$(P_T)_{\gamma\gamma} > 200.0$ GeV	22.160 ± 4.36	60.75 ± 7.70	2.800 ± 0.0260

Table 5: Cut flow for $h' \to hh \to b\bar{b}\gamma\gamma$ at $L_{\text{int}} = 3000$ fb^{-1} and $\sqrt{s} = 14$ TeV for $m_{h'} = 600$ GeV.

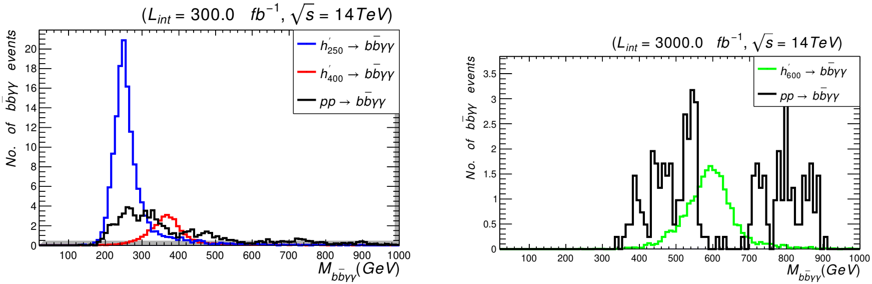

Figure 3: Left: Number of signal events for $h' \to b\bar{b}\gamma\gamma$ decays at mass $m_{h'} = 250$ GeV (blue) and 400 GeV (red) induced by ggF versus the invariant mass of the final states $b\bar{b}\gamma\gamma$, at $\sqrt{s} = 14$ TeV and $L_{\rm int} = 300$ fb^{-1} alongside with the relevant background events (black) after applying the cut flow of Tab. 4. Right: $m_{h'} = 600$ GeV (green) at $\sqrt{s} = 14$ TeV and $L_{\rm int} = 3000$ fb^{-1} alongside the background (black) after (right) applying the cut flow set of Tab. 5.

Cuts (Select)	Signal (S): $m_{h'} = 250$ GeV (400 GeV)	Background (B)	S/$\sqrt{\text{B}}$
Initial (no cut)	$728.00\ (174.00)$	79890.00	$2.58000\ (0.43000)$
$\not{H}_T > 150.0$ GeV	$58.65 \pm 7.34\ (38.20 \pm 2.01)$	247.70 ± 15.70	$2.02457 \pm 0.00790\ (1.26340 \pm 0.$

Table 6: Cut flow charts for the $h' \to ZZ \to 4\ell$ signal versus its relevant background and the corresponding number of events and significance at 3000 fb^{-1} and $\sqrt{s} = 14$ TeV for $m_{h'} = 250$ GeV, 400 GeV.

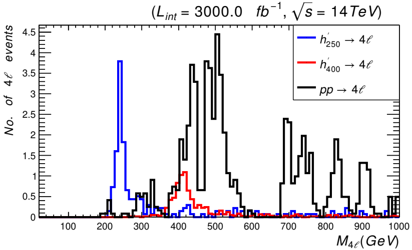

Figure 4: Number of signal events for $pp \to h' \to ZZ \to 4\ell$ decays at mass $m_{h'} = 250$ GeV (red) and 400 GeV (blue) at $\sqrt{s} = 14$ TeV and $L_{\text{int}} = 3000$ fb^{-1} with the background (black) applying the cut flow of Tab. 6.

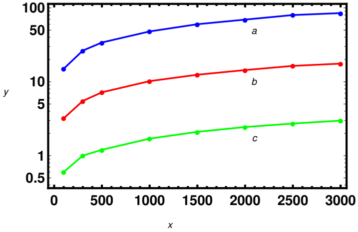

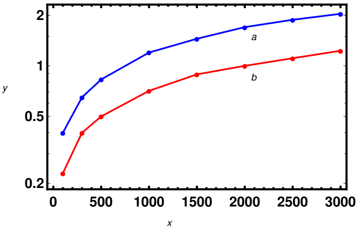

Figure 5: Left: Historical significance of $h' \to b\bar{b}\gamma\gamma$ versus L_{int} at mass $m_{h'} = 250\ , 400,\ 600$ GeV (blue/red/green). Right: Historical significance of $pp \to h' \to ZZ \to 4\ell$ signal at $m_{h'} = 250,\ 400$ GeV (blue/red).

- Recent experimental possible 4.2σ a_μ deviation from the SM [11, 1]

$$\delta a_\mu = a_\mu^{\mathsf{exp}} - a_\mu^{\mathsf{SM}} = (2.51 \pm 0.59) \times 10^{-9}. \quad (5)$$

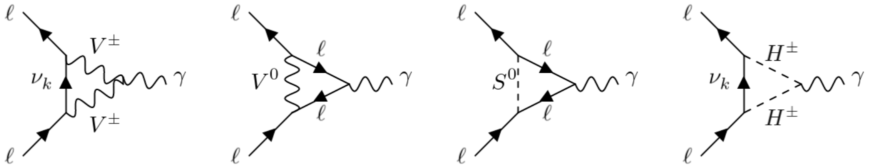

Figure 6: LRIS 1-loop a_ℓ via $\nu_k, H^{\pm}, V^{\pm} = W, W', V^0 = Z, Z', S^0 = h, A$.

- The relevant $H^{\pm}$-leptons couplings are

$$\xi_{k\ell} \simeq \frac{\sqrt{2}}{v c_{2\beta}} \sum_{i=1}^{3} U^*_{k,i+3} \left(s_{2\beta} M_{\mathsf{lp}} - M_D \right)_{\ell i}, \quad k = 4, \ldots, 9, \quad (6)$$

$$\zeta_{k\ell} \simeq \frac{\sqrt{2}}{v c_{2\beta}} \sum_{i=1}^{3} U_{ki} \left(M_{\mathsf{lp}} - s_{2\beta} M_D \right)_{i\ell}, \quad k = 1, 2, 3, \quad (7)$$

- The charged Higgs $H^\pm$ contribution to a_μ is given by

$$a_\ell^{H^\pm} = G_\mathsf{F}^\ell \, \Gamma_\gamma^{H^\pm} \sum_{k=1}^{9} \Big(|{\zeta'}_{k\ell}|^2 \, \mathcal{F}_2(x_{H^\pm}^{\nu_k}) + 2\mathrm{Re}[{\zeta'}_{k\ell}{\xi'}^*_{k\ell}] \, \mathcal{F}_1(x_{H^\pm}^{\nu_k}) \Big), \quad (8)$$

  where the couplings ${\zeta'}_{k\ell} = \frac{v}{m_{\nu_k}}\zeta_{k\ell}$ and ${\xi'}_{k\ell} = \frac{v}{m_\ell}\xi_{k\ell}$.
- The loop functions $\mathcal{F}_k$ $(k = 1, 2)$ in Eq. (8) are given by

$$\mathcal{F}_k(y) = \frac{y\mathcal{P}_k(y)}{(y-1)^{k+1}} - \frac{6y^{k+1}\log(y)}{(y-1)^{k+2}}, \quad k = 1, 2, \quad (9)$$

$$\mathcal{P}_1(y) = 3y + 3, \quad (10)$$

$$\mathcal{P}_2(y) = 2y^2 + 5y - 1. \quad (11)$$

- The charged Higgs boson contribution to the a_μ anomaly Eq. (8) can be approximated to

$$a_\ell^{H^\pm} \simeq 2G_\mathsf{F}^\ell\, \Gamma_\gamma^{H^\pm} \sum_{k=4}^{9} \mathrm{Re}[\zeta'_{k\ell}\xi'^*_{k\ell}]\; \mathcal{F}_1(x_{H^\pm}^{\nu_k}) \lesssim \frac{3\Gamma_\gamma^{H^\pm}}{8\pi^2}\; m_\ell \sum_{k=4}^{9} \frac{\zeta_{k\ell}\xi_{k\ell}}{m_{\nu_k}}. \quad (12)$$

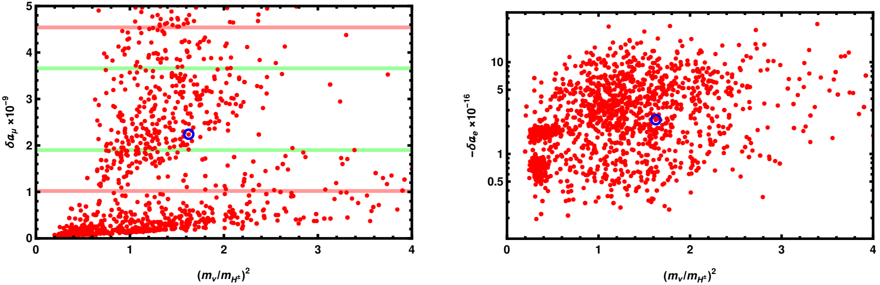

Figure 7: (Left/right) $\delta a_{\mu,e}$ with $x_{H^\pm}^{\nu_5} = m_{\nu_5}^2/m_{H^\pm}^2$. The 1σ and 2σ standard errors of measurements of a_μ are included in green and red borders. BP is encircled.

α_{32}	t_β	v_R	$Z_{31}^{H^\pm}$	$Z_{32}^{H^\pm}$	$Z_{33}^{H^\pm}$	$m_{H^\pm}$
0.0058	0.1	10000	-0.099	-0.994	0.024	545

Table 7: BP and $H^\pm$ mixing and mass for $y^s = \text{diag}(1.53 \times 10^{-2}, 9.76 \times 10^{-1}, 2.05 \times 10^{-1})$ and $\mu^s = \text{diag}(1.01 \times 10^{-5}, 3.82 \times 10^{-9}, 5.49 \times 10^{-6})$. Finally, the nonvanishing elements of the orthogonal matrix $\mathcal{R}$ are $\mathcal{R}_{13} = \mathcal{R}_{21} = \mathcal{R}_{32} = 1$.

m_{ν_1}	m_{ν_2}	m_{ν_3}	m_{ν_4}	m_{ν_5}	m_{ν_6}	m_{ν_7}	m_{ν_8}	m_{ν_9}
1.0×10^{-13}	8.5×10^{-12}	5.0×10^{-11}	108	695	1449	108	695	1449

Table 8: BP neutrino mass spectrum in GeVs.

δa_μ	$-\delta a_e$	BR$(\mu \to e\gamma)$
2.5×10^{-9}	8.1×10^{-17}	3.4×10^{-13}

Table 9: BP Observalbles $g_{\mu(e)} - 2$, BR$(\mu \to e\gamma)$ of the BP given in Tab. 8.

Matrix	$\mathcal{R}$	y^s	μ^s	y^L	$\tilde{y}^L$	y^Q	$\tilde{y}^Q$	U_{PMNS}
1, 1	0	1.53×10^{-2}	1.01×10^{-5}	-2.83×10^{-5}	3.13×10^{-4}	6.33×10^{-5}	-3.44×10^{-4}	0.8251
1, 2	0	0	0	-6.86×10^{-3}	6.86×10^{-2}	-1.49×10^{-4}	1.48×10^{-3}	0.5449
1, 3	1	0	0	-9.42×10^{-5}	9.42×10^{-4}	-3.53×10^{-4}	3.53×10^{-3}	0.1490
2, 1	1	0	0	-2.75×10^{-5}	2.75×10^{-4}	1.38×10^{-4}	-1.38×10^{-3}	−0.4554
2, 2	0	9.76×10^{-2}	3.82×10^{-9}	-3.39×10^{-2}	3.46×10^{-1}	2.27×10^{-5}	5.26×10^{-3}	0.4795
2, 3	0	0	0	5.20×10^{-5}	-5.20×10^{-4}	-4.19×10^{-3}	4.19×10^{-2}	0.7513
3, 1	0	0	0	3.93×10^{-4}	-3.93×10^{-3}	-6.08×10^{-4}	6.08×10^{-3}	0.3343
3, 2	1	0	0	-2.96×10^{-2}	2.96×10^{-1}	4.16×10^{-3}	-4.16×10^{-2}	−0.6836
3, 3	0	2.05×10^{-1}	5.49×10^{-6}	1.03×10^{-2}	-6.54×10^{-4}	-7.66×10^{-2}	9.99×10^{-1}	0.6427

Table 10: Yukawa and IS matrices BP.

$$U = \begin{pmatrix} U_{3\times3} & U_{3\times6} \\ U_{6\times3} & U_{6\times6} \end{pmatrix}^T = \left(\begin{array}{ccc|cccccc} -0.8243 & 0.4535 & -0.3389 & 0 & 0 & 0 & 0 & 0.0000 & -0.0001 \\ 0.5465 & 0.4812 & -0.6853 & 0 & 0 & 0 & 0.0009 & 0.0002 & 0 \\ -0.1468 & -0.7453 & -0.6403 & 0 & 0 & 0 & 0 & -0.1137 & 0 \\ \hline -0.0004 & -0.0003 & 0.0004 & -0.7071 & 0 & 0 & 0.7071 & 0 & 0 \\ -0.0120 & -0.0604 & -0.0517 & 0 & -0.7071 & 0 & 0 & 0.7025 & 0 \\ 0.0001 & 0.0000 & 0.0003 & 0 & 0 & 0.7071 & 0 & 0 & -0.7071 \\ -0.0004 & -0.0003 & 0.0004 & 0.7071 & 0 & 0 & 0.7071 & 0 & 0 \\ 0.0120 & 0.0604 & 0.0517 & 0 & -0.7071 & 0 & 0 & -0.7025 & 0 \\ -0.0001 & 0.0000 & 0.0000 & 0 & 0 & 0.7071 & 0 & 0 & 0.7071 \end{array}\right),$$

- Experimentally, BR$(\mu \to e\gamma) \lesssim 4.2 \times 10^{-13}$ (90%CL) [6]. LRIS $H^\pm$

$$\text{BR}(\mu \to e\gamma)_{\text{LRIS}} \lesssim \frac{9\alpha_{\text{em}}}{256\pi^4} \frac{m_\mu^5}{\Gamma_\mu} \sum_{k=4}^{9} \frac{1}{m_{\nu_k}^2} \left(\frac{\zeta_{k,e}\xi_{k,\mu}}{m_\mu} + \frac{\xi_{k,e}\zeta_{k,\mu}}{m_e} \right)^2. \qquad (14)$$

- Also, experiments make the upper bounds $R^{\text{Ti}}_{\mu\to e} \leqslant 10^{-18}$, $R^{\text{Al}}_{\mu\to e} \leqslant 10^{-16}$, $R^{\text{Au}}_{\mu\to e} \leqslant 7 \times 10^{-13}$ to the μ-e conversion rates on a nucleus (A) [12].
- The $H^\pm$ contribution to the μ-e conversion is [2, 8]

$$R^A_{\mu\to e} = \frac{32 G_{\text{F}}^2 m_\mu^5}{\Gamma^A_{\text{capt}}} \left[\left| \widetilde{C}^{pp}_{V,R} V_A^{(p)} + \widetilde{C}^{nn}_{V,R} V_A^{(n)} + \frac{1}{4} C_{D,L} D_A \right|^2 + \{L \leftrightarrow R\} \right]. \qquad (15)$$

$\Gamma^A_{\text{capt}} \sim \mathcal{O}(1-10) \times 10^6\ s^{-1}$, and $V_A^{(p)}, V_A^{(n)}, D_A \sim \mathcal{O}(10^{-2} - 10^{-1})$ for $A =$ Al, Ti, Au [12].

BR$(\mu \to e\gamma)$	$R^{\text{Al}}_{\mu\to e}$	$R^{\text{Ti}}_{\mu\to e}$	$R^{\text{Au}}_{\mu\to e}$
2.10×10^{-13}	4.10×10^{-51}	3.80×10^{-50}	4.10×10^{-49}

Table 11: LFV observables BP given in Table 8 in LRIS.

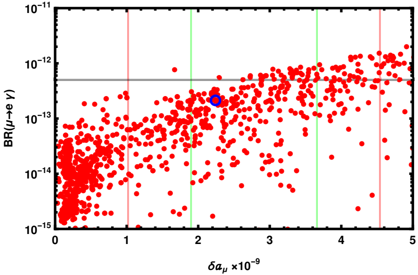

Figure 8: BR$(\mu \to e\gamma)$ versus δa_μ in LRIS. BP is encircled.

- All BPs are tested and found to satisfy the μ-e conversion experimental limits as in Table 11.

Outline

1 The LRIS Model

2 Heavy Higgs in LRIS at the LHC
- $h' \to hh \to b\bar{b}\gamma\gamma$ and $h' \to ZZ \to 4\ell$
- $H^{\pm}$ Contribution to a_μ

3 **Heavy Higgs in BLSSM Model**

4 Conclusion

- Superpotential

$$W = Y_u^{ij}\hat{u}_i^c\hat{Q}_j\cdot\hat{H}_u - Y_d^{ij}\hat{d}_i^c\hat{Q}_j\cdot\hat{H}_d - Y_e^{ij}\hat{E}_i^c\hat{L}_j\cdot\hat{H}_d + Y_\nu^{ij}\hat{N}_i^c\hat{L}_j\cdot\hat{H}_u$$
$$+ \frac{1}{2}Y_N^{ij}\hat{N}_i^c\hat{\chi}_1\hat{N}_j^c + \mu\hat{H}_u\cdot\hat{H}_d - \mu'\hat{\chi}_1\hat{\chi}_2.$$

Superfield	Spin-0	Spin-$\frac{1}{2}$	Generations	$\mathbb{G}_{\mathrm{SM}}\otimes U(1)_{B-L}$
$\hat{Q}$	$\tilde{Q}$	Q	3	$(\mathbf{3},\mathbf{2},\ \frac{1}{6},\ \frac{1}{3})$
$\hat{d}^c$	$\tilde{d}^c$	d^c	3	$(\overline{\mathbf{3}},\mathbf{1},\ \frac{1}{3},-\frac{1}{3})$
$\hat{u}^c$	$\tilde{u}^c$	u^c	3	$(\overline{\mathbf{3}},\mathbf{1},-\frac{2}{3},-\frac{1}{3})$
$\hat{L}$	$\tilde{L}$	L	3	$(\mathbf{1},\mathbf{2},-\frac{1}{2},-1)$
$\hat{E}^c$	$\tilde{e}^c$	e^c	3	$(\mathbf{1},\mathbf{1},\ 1,\ 1)$
$\hat{N}^c$	$\tilde{N}^c$	N^c	3	$(\mathbf{1},\mathbf{1},\ 0,\ 1)$
$\hat{H}_d$	H_d	$\tilde{H}_d$	1	$(\mathbf{1},\mathbf{2},-\frac{1}{2},\ 0)$
$\hat{H}_u$	H_u	$\tilde{H}_u$	1	$(\mathbf{1},\mathbf{2},\ \frac{1}{2},\ 0)$
$\hat{\chi}_1$	χ_1	$\tilde{\chi}_1$	1	$(\mathbf{1},\mathbf{1},\ 0,-2)$
$\hat{\chi}_2$	χ_2	$\tilde{\chi}_2$	1	$(\mathbf{1},\mathbf{1},\ 0,\ 2)$

- The $Z - Z'$ mixing angle is

$$\tan 2\theta' = \frac{2\tilde{g}\sqrt{g_1^2 + g_2^2}}{\tilde{g}^2 + 16(\frac{v'}{v})^2 g_{BL}^2 - g_2^2 - g_1^2} \lesssim 10^{-3}, \qquad (16)$$

where $\tilde{g}$ is the gauge mixing between $U(1)_Y$ and $U(1)_{B-L}$ and $v' = \sqrt{v_1^2 + v_2^2}$ is the $B - L$ vev.

- The Higgs potential is

$$\begin{aligned} V(H,\chi) = {} & |\mu|^2(|H_u^0|^2 + |H_d^0|^2) + |\mu'|^2(|\chi_1|^2 + |\chi_2|^2) \\ & + \frac{g^2}{8}(|H_u^0|^2 - |H_d^0|^2)^2 + \frac{g_{BL}^2}{2}(|\chi_1|^2 - |\chi_2|^2)^2 \\ & - \frac{\tilde{g} g_{BL}}{4}(|H_u^0|^2 - |H_d^0|^2)(|\chi_1|^2 - |\chi_2|^2) \\ & - m_1^2|\chi_1|^2 - m_2^2|\chi_2|^2 - B'_\mu \chi_1 \chi_2. \end{aligned}$$

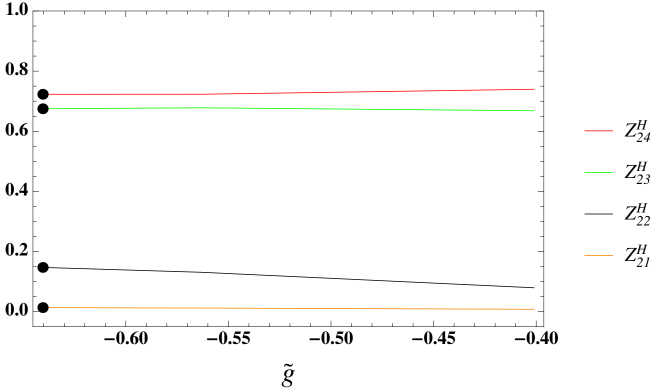

Figure 9: The Higgs mixing Z^H_{2i} $(i = 1, \ldots, 4)$ versus the gauge kinetic mixing coupling $\tilde{g}$.

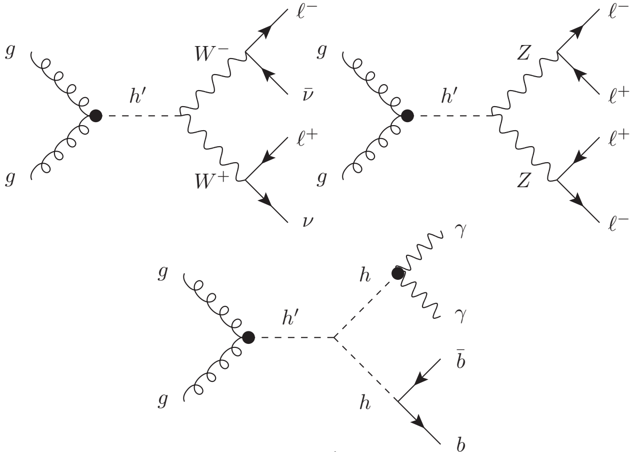

Figure 10: Feynman diagrams for h' production via ggF and decays via (from left to right) $W^+W^- \to 2\ell + \not{E}_T$, $h' \to ZZ \to 4\ell$ and $h' \to hh \to b\bar{b}\gamma\gamma$.

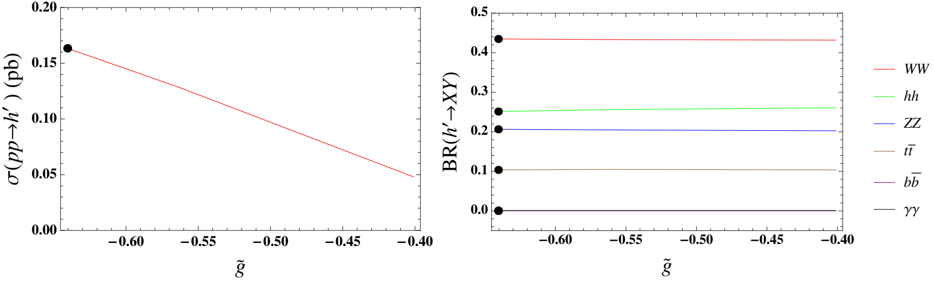

Figure 11: ggF h' production cross section at $\sqrt{s} = 14$ TeV (left) and h' decay BRs (right) versus the kinetic mixing coupling $\tilde{g}$.

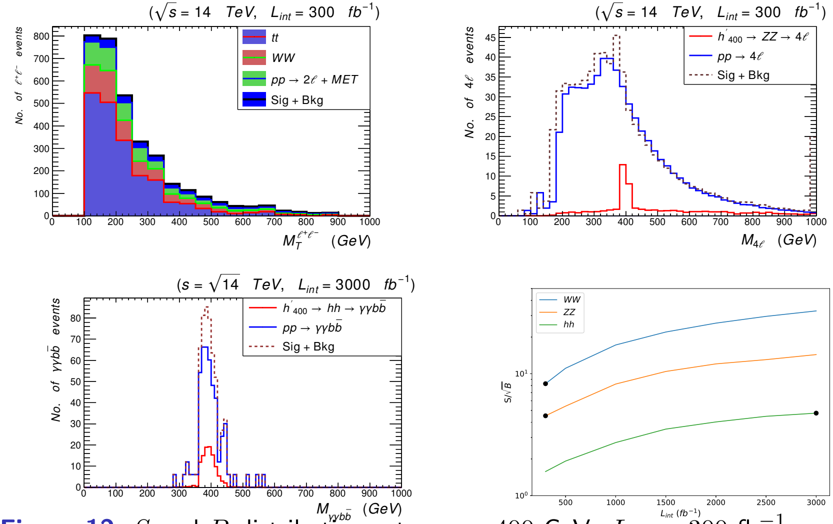

Figure 12: S and B distributions at $m_{h'} = 400$ GeV, $L_{\text{int}} = 300$ fb^{-1}.
Below-right: Historical significance.

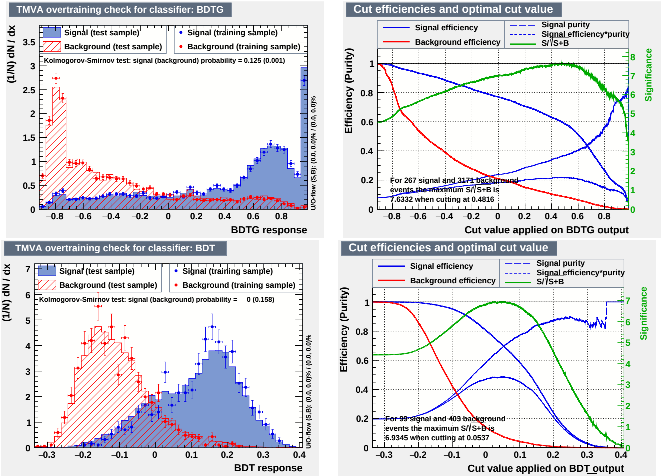

Figure 13: $H \to WW \to 2j + MET$ (up) and $H \to hh \to \gamma\gamma bb$ (down): S and B distributions, significance, correlation matrix and the ROC curves for different learning ML algorithms at $m_{h'} = 400$ GeV, $L_{\text{int}} = 300/3000\ \text{fb}^{-1}$ [15].

Outline

1 The LRIS Model

2 Heavy Higgs in LRIS at the LHC

- $h' \to hh \to b\bar{b}\gamma\gamma$ and $h' \to ZZ \to 4\ell$
- $H^{\pm}$ Contribution to a_μ

3 Heavy Higgs in BLSSM Model

4 Conclusion

- Possible signatures for heavy nonsusy Higgs bosons.
- Possible signatures for heavy susy Higgs bosons.

References I

[1] B. Abi et al.
Measurement of the Positive Muon Anomalous Magnetic Moment to 0.46 ppm.
Phys. Rev. Lett., 126(14):141801, 2021.

[2] R. Alonso, M. Dhen, M. B. Gavela, and T. Hambye.
Muon conversion to electron in nuclei in type-I seesaw models.
JHEP, 01:118, 2013.

[3] M. Ashry, K. Ezzat, and S. Khalil.
Search for Heavy Neutral Higgs Bosons at the LHC.
In Beyond Standard Model: From Theory to Experiment, 2021.

[4] M. Ashry, K. Ezzat, and S. Khalil.
Muon g-2 anomaly in a left-right model with an inverse seesaw mechanism.
Phys. Rev. D, 107(5):055044, 2023.

[5] M. Ashry, S. Khalil, and S. Moretti.
Searching for a heavy neutral CP-even Higgs boson in the BLSSM at the LHC Run 3 and HL-LHC.
Eur. Phys. J. C, 84(4):433, 2024.

[6] A. M. Baldini et al.
Search for the lepton flavour violating decay $\mu^+ \to \mathrm{e}^+\gamma$ with the full dataset of the MEG experiment.
Eur. Phys. J. C, 76(8):434, 2016.

[7] Debasish Borah, Sudhanwa Patra, and Utpal Sarkar.
TeV scale Left Right Symmetry with spontaneous D-parity breaking.
Phys.Rev., D83:035007, 2011.

References II

[8] Sacha Davidson, Yoshitaka Kuno, and Masato Yamanaka.
Selecting $\mu \to e$ conversion targets to distinguish lepton flavour-changing operators.
Phys. Lett. B, 790:380–388, 2019.

[9] K. Ezzat, M. Ashry, and S. Khalil.
Search for a heavy neutral Higgs boson in a left-right model with an inverse seesaw mechanism at the LHC.
Phys. Rev. D, 104(1):015016, 2021.

[10] M.C. Gonzalez-Garcia and J.W.F. Valle.
Fast Decaying Neutrinos and Observable Flavor Violation in a New Class of Majoron Models.
Phys. Lett. B, 216:360–366, 1989.

[11] Alexander Keshavarzi, William J. Marciano, Massimo Passera, and Alberto Sirlin.
Muon $g - 2$ and $\Delta\alpha$ connection.
Phys. Rev. D, 102(3):033002, 2020.

[12] Ryuichiro Kitano, Masafumi Koike, and Yasuhiro Okada.
Detailed calculation of lepton flavor violating muon electron conversion rate for various nuclei.
Phys. Rev. D, 66:096002, 2002.
[Erratum: Phys.Rev.D 76, 059902 (2007)].

[13] R.N. Mohapatra.
Mechanism for Understanding Small Neutrino Mass in Superstring Theories.
Phys. Rev. Lett., 56:561–563, 1986.

[14] R.N. Mohapatra and J.W.F. Valle.
Neutrino Mass and Baryon Number Nonconservation in Superstring Models.
Phys. Rev. D, 34:1642, 1986.

References III

[15] Armen Tumasyan et al.
Search for a new resonance decaying into two spin-0 bosons in a final state with two photons and two bottom quarks in proton-proton collisions at $\sqrt{s} = 13$ TeV.
10 2023.

[16] C. Weiland.
Enhanced lepton flavour violation in the supersymmetric inverse seesaw.
J. Phys. Conf. Ser., 447:012037, 2013.

Thank you!
Questions?